

High-precision calculations of highly excited and autoionizing states of the nickel atom

Sheng-Bo Niu(牛生波), Jun-Yao Zhang(张钧尧), Rui Jin(金锐), and Yi-Zhi Qu(屈一至)
Citation: Chin. Phys. B, 2026, 35 (**6**): 063101. DOI: 10.1088/1674-1056/ae2a01
http://cpb.iphy.ac.cn; http://iopscience.iop.org/cpb

What follows is a list of articles you may be interested in

All-electron basis sets for H to Xe specific for ZORA calculations: Applications in atoms and molecules

C. S. Gomes, F. E. Jorge, and A. Canal Neto
Chin. Phys. B, 2024, 33 (**8**): 083101. DOI: 10.1088/1674-1056/ad4bbe

Benchmarking calculations of excitation energies and transition properties with spectroscopic accuracy of highly charged ions used for the fusion plasma and astrophysical plasma

Chunyu Zhang(张春雨), Kai Wang(王凯), Ran Si(司然), Jinqing Li(李金晴), Changxian Song(宋昌仙), Sijie Wu(吴思捷), Bishuang Yan(严碧霜), and Chongyang Chen(陈重阳)
Chin. Phys. B, 2023, 32 (**11**): 113102. DOI: 10.1088/1674-1056/acef07

Mutual neutralization in low-energy collisions of $Na^+ + H^-$ ions

Kun Wang(王堃), Chuan Dong(董川), Yizhi Qu(屈一至), Yong Wu(吴勇), Xiaohe Lin(林晓贺), and Robert J. Buenker
Chin. Phys. B, 2023, 32 (**8**): 083103. DOI: 10.1088/1674-1056/acd624

Spectroscopy and scattering matrices with nitrogen atom: Rydberg states and optical oscillator strengths

Yuhao Zhu(朱宇豪), Rui Jin(金锐), Yong Wu(吴勇), and Jianguo Wang(王建国)
Chin. Phys. B, 2022, 31 (**4**): 043103. DOI: 10.1088/1674-1056/ac1f05

Theoretical study of the radiative decay processes in $H^+(D^+, T^+)$-Be collisions

Huilin Wei(魏惠琳), Xiaojun Liu(刘晓军)
Chin. Phys. B, 2018, 27 (**12**): 123101. DOI: 10.1088/1674-1056/27/12/123101

DATA PAPER

High-precision calculations of highly excited and autoionizing states of the nickel atom

Sheng-Bo Niu(牛生波)[1], Jun-Yao Zhang(张钧尧)[2,3], Rui Jin(金锐)[4,†], and Yi-Zhi Qu(屈一至)[1,‡]

[1] *School of Optoelectronics, University of Chinese Academy of Sciences, Beijing* 100049, *China*
[2] *National Key Laboratory of Particle Transport and Separation Technology, Tianjin* 300180, *China*
[3] *Research Institute of Physical and Chemical Engineering of Nuclear Industry, Tianjin* 300180, *China*
[4] *National Key Laboratory of Computational Physics, Institute of Applied Physics and Computational Mathematics, Beijing* 100088, *China*

(Received 21 October 2025; revised manuscript received 23 November 2025; accepted manuscript online 9 December 2025)

High-precision atomic data, including highly excited energy levels and their lifetimes, as well as autoionizing states, are essential for astrophysics, materials science, and energy research applications. Despite the increasing demand for high-precision databases, the availability of data concerning complex transition-metal atoms remains limited. In this work, we present a systematic high-precision theoretical study of highly excited and autoionizing states of the nickel atom for $J^{\pi} = 4^{-}$ symmetry, considering the indispensable correlation effects between bound and continuum configurations. Calculations for discrete highly excited states and autoionizing states are conducted under the same theoretical scheme, which employs the relativistic multichannel theory (RMCT), to obtain an eigenchannel scattering matrix that varies smoothly over a wide energy region. The scattering matrix is then used with the multichannel quantum defect theory (MQDT) to semi-analytically obtain highly excited states and autoionizing states. Excellent agreement is achieved between the theoretical results and existing experimental discrete levels with a maximum of 0.02% deviation. An abnormal lifetime variation of the autoionizing states along the same series is observed. The resonance energy, lifetime, and assignment of autoionizing states are systematically presented for the first time, with the objective of contributing to the fields of astrophysics, materials science, and energy research. The datasets presented in this paper, including the energy levels and lifetimes of autoionizing states, are openly available at https://doi.org/10.57760/sciencedb.j00113.00279.

Keywords: multichannel quantum defect theory, highly excited states, autoionizing states, high precision

PACS: 31.15.ae, 31.15.ag, 31.15.V–

DOI: 10.1088/1674-1056/ae2a01 **CSTR:** 32038.14.CPB.ae2a01

1. Introduction

Electronic structures and dynamic properties of atoms in ground, excited, and autoionizing states play a crucial role in studies of astrophysics, materials science, and energy research. Atomic spectral lines have long been used for the diagnostics of astro-objects such as nebular and stellar objects and planetary atmospheres. Opacity is the key physical quantity in the study of stellar structures and radiative transfer. It is known to play an important role in constructing stellar evolution models and in the analysis of the interstellar medium.[1,2] The opacity of stellar systems is largely influenced by the chemical elements present in their atmospheres, especially the iron-group elements such as iron (Fe), cobalt (Co), and nickel (Ni), which significantly affect the star's absorption features in the vacuum ultraviolet (VUV) region.[3–9] In addition to the bound–bound transitions, the importance of autoionizing states in the study of opacities has received significant recognition.[10,11] Besides astrophysics, accurate atomic nickel data are also essential for laboratory and industrial plasmas, synchrotron-based photoionization studies, and precision calibration of VUV spectrometers, where unresolved autoionizing features bias instrument response functions and absolute cross-section measurements.[9,12,13] In the context of magnetic confinement fusion, nickel is a key material for divertors.[14] Therefore, it is important to study its spectral and thermal properties in extreme plasma environments. However, both experimental and theoretical data for nickel remain limited, particularly for highly excited Rydberg states and autoionization resonances.

The scarcity of electronic structure and dynamical property data for highly excited autoionizing states of the nickel atom is due to the complexity brought about by its open-shell structure and the strong correlation effects related to the orbital competition between 4s- and 3d-waves. In addition, the strong coupling of bound and continuum configurations becomes indispensable for high-precision theoretical calculations on the states of interest.[9,12,15] These many-body effects lead to multiple competing ionization channels in the VUV, complicating line identification and the assignment of resonance series.[15,16]

†Corresponding author. E-mail: jin_rui@iapcm.ac.cn
‡Corresponding author. E-mail: yzqu@ucas.ac.cn

© 2026 Chinese Physical Society and IOP Publishing Ltd. All rights, including for text and data mining, AI training, and similar technologies, are reserved.

While experimental methods have made some progress in measuring nickel's VUV spectrum, they have not been able to resolve the fine structure of nickel's autoionization resonances.[9,12,15] Therefore, theoretical calculation has become an essential complement to experiments.[13,15,16] Various perturbative and nonperturbative theoretical methods have been developed for high-precision calculations of atomic and molecular electronic structures. For instance, many-body perturbation theory (MBPT) and configuration interaction (CI) have been employed to predict nickel's spectra. However, due to the complexity of many-body effects and the lack of bound–continuum configuration interactions, these methods still exhibit significant discrepancies with experimental results.[16–18] Therefore, there is a pressing need for novel high-precision theoretical studies on the highly excited and autoionizing states of the nickel atom.

Multichannel theories have been developed to treat bound–continuum configuration interactions in scattering, photoionization, and autoionization dynamics. In multichannel theories, the short-range scattering matrix, or equivalently the reaction matrix, is obtained as the key physical parameter, with which various physical observables such as energy levels and cross sections can be obtained. A special category of multichannel theories, based on the eigenchannel scheme, produces eigenchannel scattering matrices that are proven to possess analytical properties, meaning they vary smoothly with energy across the ionization thresholds.[19–23] Therefore, the smooth scattering matrix parameters calculated at a few energy grids are sufficient to capture all the incorporated physics. In this work, the relativistic multichannel theory (RMCT)[24–26] is employed to calculate the eigenchannel scattering matrix parameters, which provide flexible control of various bound–bound configuration interactions as well as bound and continuum ones. The calculated scattering matrices are then used with the multichannel quantum defect theory (MQDT) procedure to obtain infinitely many discrete and autoionization states.[19–23] Besides the huge efficiency benefit, the eigenchannel scheme provides a clearer physical understanding as well as easier assignment of the energy levels and resonances.

In this work, we demonstrate the potential of the eigenchannel scheme in the high-precision calculation of highly excited and autoionizing states for complex transition atoms, using the nickel atom with $J^{\pi} = 4^{-}$ symmetry as an example. Excellent agreement with existing experimental values is achieved. The anomalous lifetime of autoionizing states is studied to reveal the interesting bound–continuum correlation effects. This work is organized as follows. We first briefly introduce the calculation of scattering matrices in both the bound and continuum energy regions in Subsection 2.1. Subsequently, we demonstrate the graphical semi-analytical MQDT procedure to obtain the highly excited and autoionizing states in Subsections 2.2 and 2.3, respectively. Finally, a short summary is given in Section 3.

2. Theoretical models and calculation results

2.1. Scattering matrix parameters

The complex electronic correlation effects can be faithfully captured by the energetically smooth-varying eigenchannel short-range scattering matrices.[24–27] These matrices are routinely supplied to MQDT procedures[24,25] to retrieve infinitely many Rydberg states as well as autoionization states encompassed therein. The short-range scattering matrices are calculated in the relativistic multichannel theory (RMCT) framework.[24,25] The working formulation of RMCT has been introduced throughout its long history of development and applications, for example;[24–26] therefore, we focus our theoretical description merely on modeling the correlations in the nickel atom of interest. In our case, the important correlation of core excitation and breathing effects is incorporated by including various core states in the RMCT calculations to obtain the scattering matrix parameters.

The RMCT can be regarded as an extension of the traditional configuration interaction (CI) method by including the Rydberg states and the continuum states interaction.[24,26] It directly aims to calculate the MQDT parameters (μ_α, $U_{i\alpha}$). The bound and continuum configuration wavefunctions (Φ_n, $\Phi_{j\varepsilon}$) are constructed as antisymmetrized product-type wavefunctions of single-electron wavefunctions, obtained from the relativistic self-consistent field method. The wavefunctions of energy eigenstates can then be expressed as[24–26]

$$\Psi(E,i) = \sum_n A_n(E,i)\Phi_n + \sum_j \int_{\varepsilon_c} B_{j\varepsilon}(E,i)\Phi_{j\varepsilon}\,\mathrm{d}\varepsilon, \tag{1}$$

where j indexes each ionization channel. The coefficients of the linear superposition, A_n and $B_{j\varepsilon}(E,i)$, can be expressed as

$$A_n(E,i) = \frac{K_{n,iE}}{(E-E_n^0)} \cdot N(E,i), \tag{2}$$

$$B_{j\epsilon}(E,i) = \left[\frac{K_{j\epsilon,iE}}{(E-\epsilon)} + \delta_{ji}\cdot\delta(\epsilon - E)\right]\cdot N(E,i) \tag{3}$$

in terms of the K matrix. By solving the Lippmann–Schwinger integral equation and diagonalizing the on-shell K matrix, the physical parameters of MQDT, including the eigenchannel phase shifts μ_α and the transformation matrix $U_{i\alpha}$,[24,25] are directly obtained.

Before proceeding to the practical details of modeling the correlation effects of nickel atoms, a brief introduction to the concept of ionization and eigenchannels is needed. In the framework of MQDT, the ionization channel is defined as the close-coupling asymptotic wavefunction for the ionization dynamics of the $N+1$ electronic atomic system, and naturally, it is described by a jj-coupled wavefunction of the target ion

and continuum electrons. Each of the ionization channels possesses a phase shift due to the time delay of the scattering of the continuum wavefunction with the tightly bound target ion. The eigenchannel is a special choice of representation that combines the ionization channels with the same phase shift — so-called eigenphase shift. In this representation, the scattering matrix possesses analytical properties and varies smoothly with energy.[21–23,27] The diagonalization of the scattering matrix provides us with n eigenchannel phase shifts μ_α, and an $n \times n$ transformation matrix $U_{i\alpha}$ that represents the interchannel interaction strength.[19–23] With the pair of scattering matrix parameters, μ_α and $U_{i\alpha}$, one can obtain infinitely many discrete and autoionizing states and readily compare them with experimentally observed values.

Recently, Zhang *et al.* systematically investigated the odd-parity autoionizing states of nickel using a three-color three-step laser resonance ionization mass spectrometry technique. Through cross-scanning of eight second excited state energy levels, 170 energy level data points within the range of 3980.33–7080.33 cm^{-1} were reported.[28] By scanning three excited state energy levels in the range of 7080.33–7980.33 cm^{-1}, 103 energy level data points were also discovered, among which the total angular momentum of 41 energy levels was determined to be 4.[29]

Table 1. Physical channels and corresponding eigenchannels for the Ni system with $J^\pi = 4^-$ symmetry in the energy range from -3500 cm^{-1} to -1000 cm^{-1}.

Index	1	2	3	4
Physical channels	$(3d^9)^2D_{5/2}\,np_{3/2}$	$3d^8(^3F)4s^4F_{9/2}\,np_{3/2}$	$3d^8(^3F)4s^4F_{5/2}\,np_{3/2}$	$3d^8(^3F)4s^4F_{7/2}\,np_{1/2}$
Eigenchannels	$^3F_4$	$^3G_4$	$^1G_4$	$^3F_4$
Index	5	6	7	8
Physical channels	$3d^8(^3F)4s^4F_{7/2}\,np_{3/2}$	$3d^8(^3F)4s^2F_{7/2}\,np_{1/2}$	$3d^8(^3F)4s^4F_{9/2}\,np_{1/2}$	$3d^8(^1D)4s^2D_{5/2}\,np_{3/2}$
Eigenchannels	$^3F_4$	$^5D_4$	$^5G_4$	$^3F_4$
Index	9	10	11	12
Physical channels	$3d^8(^3F)4s^2F_{7/2}\,np_{3/2}$	$(3d^9)^2D_{5/2}\,nf_{5/2}$	$(3d^9)^2D_{3/2}\,nf_{5/2}$	$3d^8(^3P)4s^4P_{5/2}\,np_{3/2}$
Eigenchannels	$^5F_4$	$^3H_4$	$^3G_4$	$^5D_4$
Index	13	14	15	
Physical channels	$(3d^9)^2D_{5/2}\,nf_{7/2}$	$(3d^9)^2D_{3/2}\,nf_{7/2}$	$3d^8(^3F)4s^2F_{5/2}\,np_{3/2}$	
Eigenchannels	$^3F_4$	$^1G_4$	$^3G_4$	

Table 2. Physical channels and corresponding eigenchannels for the Ni system with $J^\pi = 4^-$ symmetry in the energy range from 6650 cm^{-1} to 7300 cm^{-1}.

Index	1	2	3	4
Physical channels	$3d^9\,^2D_{5/2}\,np_{3/2}$	$3d^8(^3F)4s^4F_{9/2}\,np_{3/2}$	$3d^8(^1G)4s^2G_{7/2}\,np_{1/2}$	$3d^8(^1G)4s^2G_{9/2}\,np_{1/2}$
Eigenchannels	$^3F_4$	$^3G_4$	$^3F_4$	$^1G_4$
Index	5	6	7	8
Physical channels	$3d^8(^3F)4s^4F_{7/2}\,np_{3/2}$	$3d^8(^3F)4s^2F_{7/2}\,np_{1/2}$	$3d^8(^3F)4s^4F_{9/2}\,np_{1/2}$	$3d^8(^1D)4s^2D_{5/2}\,np_{3/2}$
Eigenchannels	$^3F_4$	$^5D_4$	$^5G_4$	$^3F_4$
Index	9	10	11	12
Physical channels	$3d^8(^3F)4s^2F_{7/2}\,np_{3/2}$	$3d^9\,^2D_{5/2}\,nf_{5/2}$	$3d^8(^3F)4s^2F_{7/2}\,nf_{5/2}$	$3d^8(^1G)4s^2G_{7/2}\,np_{3/2}$
Eigenchannels	$^5F_4$	$^3H_4$	$^1G_4$	$^3H_4$
Index	13	14	15	16
Physical channels	$3d^8(^3F)4s^2F_{7/2}\,nf_{7/2}$	$3d^8(^3F)4s^4F_{9/2}\,nf_{7/2}$	$3d^8(^3F)4s^4F_{7/2}\,np_{1/2}$	$3d^9\,^2D_{5/2}\,nf_{7/2}$
Eigenchannels	$^3G_4$	$^5D_4$	$^3F_4$	$^3F_4$
Index	17	18	19	20
Physical channels	$3d^9\,^2D_{3/2}\,nf_{5/2}$	$3d^8(^3P)4s^4P_{5/2}\,np_{3/2}$	$3d^8(^3F)4s^4F_{5/2}\,np_{3/2}$	$3d^9\,^2D_{3/2}\,nf_{7/2}$
Eigenchannels	$^3G_4$	$^5D_4$	$^1G_4$	$^1G_4$
Index	21	22	23	24
Physical channels	$3d^8(^3F)4s^4F_{9/2}\,nf_{5/2}$	$3d^8(^1G)4s^2G_{9/2}\,np_{3/2}$	$3d^8(^3F)4s^2F_{5/2}\,np_{3/2}$	$3d^8(^3F)4s^4F_{7/2}\,nf_{5/2}$
Eigenchannels	$^5I_4$	$^3G_4$	$^3G_4$	$^5H_4$
Index	25	26	27	28
Physical channels	$3d^8(^3F)4s^4F_{5/2}\,nf_{7/2}$	$3d^8(^3F)4s^4F_{7/2}\,nf_{7/2}$	$3d^8(^3F)4s^4F_{5/2}\,nf_{5/2}$	$3d^8(^3F)4s\,^4F_{3/2}\,nf_{5/2}$
Eigenchannels	$^3G_4$	$^5G_4$	$^3H_4$	$^3F_4$
Index	29			
Physical channels	$3d^8(^3F)4s^4F_{3/2}\,nf_{7/2}$			
Eigenchannels	$^5F_4$			

In this work, we focus on the Rydberg series below the first ionization threshold and the autoionization series between the second and third ionization thresholds of Ni atoms with $J^\pi = 4^-$ symmetry. Detailed calculations were performed for the Rydberg series within -3700 cm^{-1} to -1000 cm^{-1} with 15 channels from nine ionization thresholds, and for

the autoionization series within 6650 cm^{-1} to 7300 cm^{-1} with 29 channels from 12 thresholds, as shown in Tables 1 and 2, respectively. Both ionization channels labeled in the jj-coupling scheme and eigenchannels labeled in the LS coupling scheme are listed. In our RMCT calculation, 48 channels from 17 ionization thresholds, namely, Ni^+ $(3d^9)\,^2D_{5/2,3/2}$, $(3d^8(^3F)4s)\,^4F_{9/2,7/2,5/2,3/2}$, $(3d^8(^3F)4s)\,^2F_{7/2,5/2}$, $(3d^8(^3P)4s)\,^4P_{5/2,3/2,1/2}$, $(3d^8(^1D)4s)\,^2D_{3/2,5/2}$, $(3d^8(^3P)4s)\,^2P_{3/2,1/2}$, $(3d^8(^1G)4s)\,^2G_{9/2,7/2}$, and $(3d^8(^1S)4s)\,^1S_{1/2}$, are included.

The scattering matrix parameters containing the key electronic correlation effects for the nickel atom with $J^\pi = 4^-$ symmetry are obtained employing the RMCT method. As shown in Fig. 1, both eigen quantum defects μ_α and Euler angles θ_k in the bound (from -3500 cm^{-1} to -1000 cm^{-1}) and autoionization (from 6650 cm^{-1} to 7300 cm^{-1}) energy regions of interest display great analytical properties.[21–23] As shown in subfigures (a) and (c), the quantum defects of eigenchannels associated with p-waves are near (0.1–0.3 or equivalently 0.7–0.9), in sharp contrast to those of f-waves near 0 or 1. This phenomenon can be explained by the heavier orbital penetration of the p-wave than that of the f-wave, suggesting the correctness of our channel assignment. The Euler angles representing the channel transformation matrix are suitable measures of the interaction strength between corresponding channels.[21,22] The more they deviate from 0, the stronger the interaction. For instance, in Fig. 1(b), the angle $\theta_{7,8} \approx 0.185\pi$ (indicated by the pink curve) between the seventh channel $|3d^8(^3F)4s\,^4F_{9/2}\,np_{1/2}\,^5G_4\rangle F)$ and the eighth channel $|3d^8(^1D)4s\,^2D_{5/2}\,np_{3/2}\,^3F_4\rangle$ demonstrates strong coupling between the channels. In contrast, weaker couplings are indicated by $\theta_{2,7} \approx -0.018\pi$ between the 2nd channel $|3d^8(^3F)4s\,^4F_{9/2}\,np_{3/2}\,^3G_4\rangle$ and the 7th channel $|3d^8(^3F)4s\,^4F_{9/2}\,np_{1/2}\,^5G_4\rangle$, and by $\theta_{12,15} \approx -0.104\pi$ between the 12th channel $|3d^8(^3P)4s\,^4F_{5/2}\,np_{3/2}\,^5D_4\rangle$ and the 15th channel $|3d^8(^3F)4s\,^2F_{5/2}\,np_{3/2}\,^3G_4\rangle$. These well-behaving scattering matrix parameters are then used with the MQDT procedure to obtain accurate highly excited Rydberg and autoionizing states, as shown in the subsequent subsection.

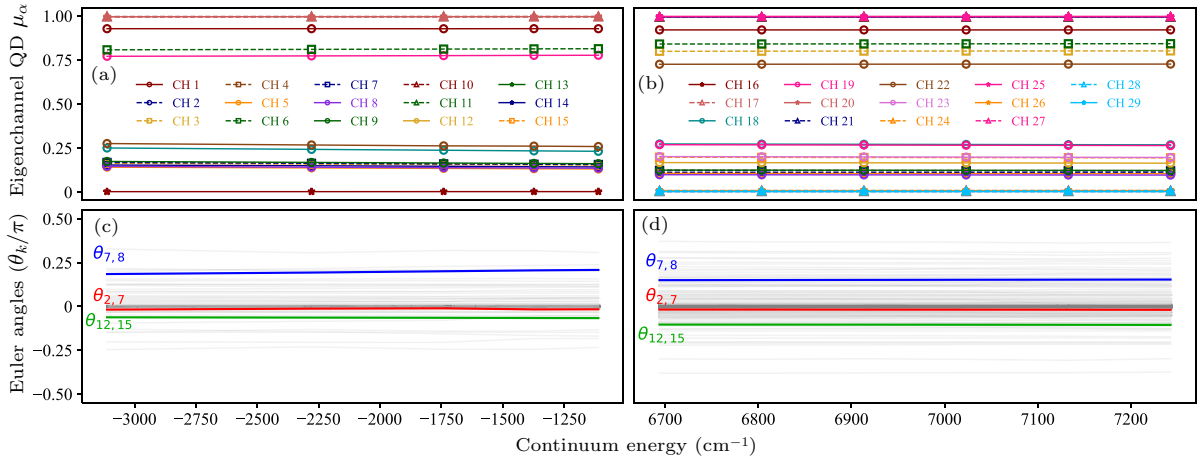


Fig. 1. Scattering matrix parameters of Ni I system with $J^\pi = 4^-$ in both discrete and autoionization energy regions. (a), (b) Eigen-quantum defects μ_α in the discrete energy region (-3500 $cm^{-1} < E < -1000$ cm^{-1}) and autoionization energy region (6650 $cm^{-1} < E <$ 7300 cm^{-1}), respectively. The channel labels correspond to the coupled channels listed in Tables 1 and 2. (c), (d) Euler angles θ_k representing transformation matrix $U_{i\alpha}$ in corresponding energy regions. The angle value indicates the interaction strengths between channels, for instance, in (b) the angle between the strongly interacting seventh channel, $|3d^8(^3F)4s\,^4F_{9/2}\,np_{3/2}\,^3G_4\rangle$, and eighth one, $|3d^8(^3F)4s\,^4F_{9/2}\,np_{1/2}\,^5G_4\rangle$, highlighted as a pink curve at $\theta_{7,8} \approx 0.185\pi$. Both the eigenchannel quantum defects and Euler angles vary smoothly with energy, demonstrating energetical analytical properties of short-range scattering matrices.

2.2. Calculation of discrete energy levels

The MQDT framework is a standard technique in atomic and molecular studies. However, a brief introduction is still necessary to facilitate further discussion in our special eigenchannel representation. Since the correlation and exchange effects are short range, the asymptotic form of the eigenchannel wavefunction is a linear combination of the regular and irregular Coulomb wave pair for each ionization channel, which reads[19–23,30,31]

$$\Psi_\alpha^{J\pi} = \sum_{i=1}^{N} \Phi_i U_{i\alpha} (\mathrm{f}_i \cos\pi\mu_\alpha - g_i \sin\pi\mu_\alpha) \quad r \to \infty, \tag{4}$$

where f_i and g_i are regular and irregular Coulomb functions, respectively, and Φ_i represents the channel wavefunction. The wave functions of physical states (energy eigenstates) are then expressed as a linear combination of eigenchannel wave functions[19–23,30,31]

$$\Psi^{J\pi}(E) = \sum_\alpha A_\alpha \Psi_\alpha^{J\pi}(E), \tag{5}$$

with the mixing coefficients A_α determined by various asymptotic boundary conditions.[19–23] For bound states, all channels are closed, and the asymptotic boundary conditions require

$$\sum_\alpha U_{i\alpha} \sin\pi(\nu_i + \mu_\alpha) A_\alpha^\rho = 0 \quad \text{for all } i, \tag{6}$$

and the effective principal quantum numbers, ν_i, are defined as

$$E^2 = I_i^2 - q^2/\nu_i^2 \quad \text{in Ry}, \tag{7}$$

where I_i and q are the ionization threshold and charge of the target ion, respectively. The system of linear Eq. (6) has the following compatibility condition:

$$\begin{aligned} F(\{x_i\},\{U_{i\alpha},\mu_\alpha\}) &= \det[U_{i\alpha}\sin\pi(x_i+\mu_\alpha)] \\ &= \det(F_{i\alpha}) = 0. \end{aligned} \tag{8}$$

The simultaneous set of $N+1$ equations, Eqs. (7) and (8), is sufficient to uniquely determine the $N+1$ unknown variables in the problem (N ν_i and one E), by means of the direct substitution–elimination method. However, this approach is not particularly convenient for systematically examining level characteristics or for validating the accuracy of the calculations against precise spectroscopic data. Instead, graphical semi-analytical methods like the Lu–Fano plot[20] for two thresholds and the "projected high dimensional quantum-defect graph (symmetrized)" (JHANGZ plot) method for multi-threshold[23] are used. These semi-analytical methods enable a systematic visual comparison of theoretical results with experimental data, with the effective quantum defect used to represent energy positions. They allow one to readily check and/or calibrate an ab initio calculated scattering matrix. In addition, the complex overlapping resonances can be systematically analyzed using the JHANGZ plot. A detailed discussion of the JHANGZ plot can be found in Ref. [23]. In short, we can use energy constraints from Eq. (7) to project the multiple unknown variables in Eq. (8) onto a two-dimensional subspace. There is a parameter, I_x, representing one of the ionization thresholds to control the general geometric structure of this plot. Channels associated with thresholds higher than I_x must obey discrete boundary conditions and thus behave as resonances. The corresponding effective principal quantum number corresponding to I_x will be denoted as ν_x via Eq. (7). The other channels associated with thresholds lower than I_x are the analytical continuation of the opened channels (so-called collisional channels[20]) in the continuum energy region, which thus obey travelling-wave boundary conditions. The associated collisional scattering phase shifts obtained from Eq. (8) are depicted as smooth horizontal curves, which closely resemble the relevant eigenchannel quantum defects, despite being perturbed locally near the resonances. In principle, one can choose any two effective principal quantum numbers to span the projected subspace. However, some choices of abscissa and ordinate (determined by one) do simplify the physical analysis and facilitate checking/calibrating eigenchannel scattering matrices with experiments and assignments. Taking $J^\pi = 4^-$ as an example, we choose the effective principal quantum number associated with the second one, $(3d^9)^2D_{3/2}$, to show moderately dense resonances.

Due to the complex electronic structure of the Ni atom, theoretical calculations and experimental measurements of its energy levels are relatively scarce, especially for the high-lying Rydberg series. To obtain all high-precision energy levels in the Rydberg series of interest, we used the MQDT parameters from Fig. 1 and systematically calculated the relevant energy levels for three Rydberg series. In Fig. 2 (JHANGZ plot), nine branch curves with different colors and two different line styles, determined by the mixing coefficients, A_α, of the eigenchannel wavefunctions, are presented (the labels in the figure are consistent with those in Fig. 1). These curves represent the effective phase shifts of the different eigenchannels obtained by solving Eq. (8). The second threshold $3d^{9\,2}D_{3/2}$ is chosen as I_x so that the f-waves associated with the first threshold $3d^{9\,2}D_{5/2}$ are all smooth horizontal curves instead of being sharp resonances (other f-waves associated with higher thresholds are not available in the bound energy region, due to the energy restraint $\varepsilon > -1/l^2$ of Coulomb wavefunctions[20]). This choice of continuation of the opened channel greatly reduces the effort to scan the resonant structures. The actual physical states are restricted by the Rydberg energy relations for the effective quantum number ν_x associated with the first threshold, denoted as I_y. The gray dashed line marks the energy relationship $I_x - 1/\nu_x^2 = I_y - 1/\nu_y^2$, according to Eq. (7). The intersections of these curves correspond to the energy levels of the autoionizing series. Four prominent horizontal lines are found near effective quantum defects (equivalent to the modulo of the negative effective principal quantum number shown on the y-axis) at 0 or 1, corresponding to four distinct Rydberg f-wave series: $3d^{9\,2}D_{3/2}\,nf_{5/2}$, $3d^{9\,2}D_{3/2}\,nf_{7/2}$, $3d^{9\,2}D_{5/2}\,nf_{5/2}$ and $3d^{9\,2}D_{5/2}\,nf_{7/2}$ (solid and dashed lines in deep and light red). Conversely, the two p-channels associated with higher thresholds $3d^{9\,2}F_{5/2,7/2}$ are projected into two resonant structures shown as the yellow dashed line near $\nu_x = 4.91$ (for $3d^8(^3F)4s^4F_{7/2}p_{1/2}$) and the pink line near $\nu_x = 6.83$ (for $3d^8(^3F)4s^4F_{5/2}p_{3/2}$). Both channels are coupled to the $3d^{9\,2}D_{5/2}\,np_{3/2}$ channel, and the latter resonance is much wider and smoother than the first one. This contrast can be explained as follows. The continuum channel $3d^{9\,2}D_{5/2}\,np_{3/2}$ shares the same $p_{3/2}$ scattering wave with the latter resonant channel, which leads to even stronger correlation interaction. Our theoretically calculated levels, marked as hollow symbols, show excellent agreement with available experimental measurements marked as solid symbols. To highlight the comparison with experimental data,[12] a zoomed-in view of the $8.0 \le \nu_x \le 8.5$ energy region is shown in the inset figure. For levels with $\nu < 8.25$, the maximum deviation from

the experimental data by Kessler *et al.*[12] is found to be less than 0.0002%; for $\nu < 8.25$, despite the significant increase in experimental error bars, the maximum error of the calculated energy levels remains below 0.0182%, and all results lie within the experimental uncertainty range. These results demonstrate that the MQDT theory can accurately describe the fine structure, resonance behavior, and inter-channel coupling effects of the high-lying Rydberg series of Ni atoms. More importantly, the analytical property of the short-range scattering matrix guarantees the MQDT theory as a very reliable predictive tool for understanding the excited-state properties of strongly correlated transition metal atoms.

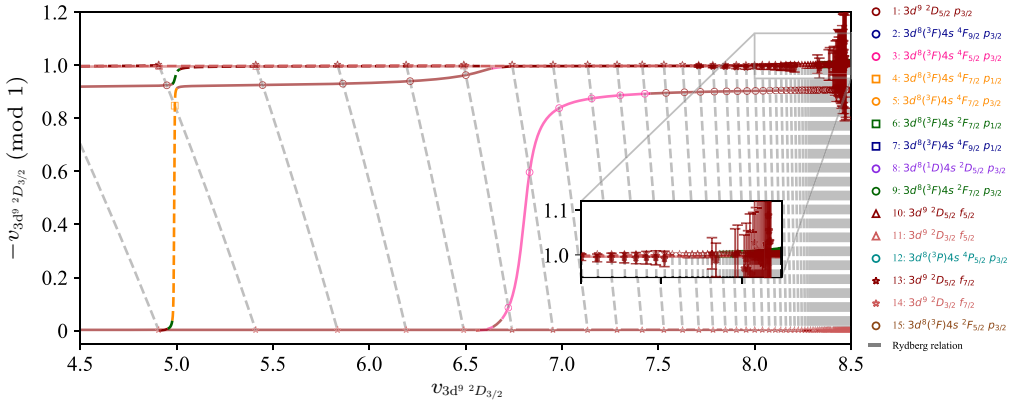


Fig. 2. Graphical solution of the MQDT equations for the Ni system in the discrete energy region, using scattering matrix parameters shown in Figs. 1(a) and 1(c). Colored curves represent solutions of Eq. (6); the theoretical physical states are obtained at the intersections (solid symbols) with the Rydberg energy relation Eq. (7) (grey segmented lines between $3d^9\,^2D_{3/2}$ and $3d^9\,^2D_{5/2}$). Excellent agreement with experiment levels[12] (opened symbols) is achieved for low-lying Rydberg states, despite large experimental uncertainties for the levels near the threshold ("mod 1" means modulo 1 operation.[20,23]).

2.3. Properties of the autoionization states

Similar to the MQDT procedure applied to the discrete energy region, autoionizing states can also be readily obtained by the semi-analytical graphical method. The difference lies in the fact that, in the autoionization region, some channels are closed while others are open. From the smooth MQDT parameters shown in Figs. 1(b) and 1(d), we can readily get resonant scattering matrices for autoionization with the channel projection method,[27] from which we can obtain all related autoionization quantities.[32–38] The MQDT equations under the new complicated boundary condition in the autoionization region should now be modified. Let us denote the number of channels that satisfy the closed channel boundary condition as N_c and the open channels as N_o; thus, the asymptotic boundary conditions require

$$\sum_\alpha U_{i\alpha}\sin\pi(\nu_i+\mu_\alpha)A^\rho_\alpha = 0 \ \text{ for } N_c \text{ closed } i, \tag{9a}$$

$$\sum_\alpha U_{i\alpha}\sin\pi(-\tau^\rho+\mu_\alpha)A^\rho_\alpha = 0 \ \text{ for } N_o \text{ opened } i, \tag{9b}$$

with N_c effective principal quantum numbers ν_i [see Eq. (8) and τ^ρ the ρ'th eigenchannel quantum defect for N_o open channels (i.e., collisional phase shift)]. The MQDT equation [Eq. (9)] is now generalized as

$$\begin{aligned} F(\{x_i\},\{U_{i\alpha},\mu_\alpha\}) &= \det[U_{i\alpha}\sin\pi(x_i+\mu_\alpha)] \\ &= \det(F_{i\alpha}) = 0, \end{aligned} \tag{10}$$

where $x_i = \nu_i$ for $i \subset N_c$ closed channels, and $x_i = -\tau^\rho$ for $i \subset N_o$ open channels. The solutions of Eqs. (7) and (10) will lead to N_o resonant eigen phase shifts $\pi\tau^\rho$, from which various properties (resonance positions, widths, etc.) of the autoionizing states can be obtained.[35,37]

The MQDT procedure is employed to study the densely overlapping autoionization states of the nickel atom based on the physical parameters from Figs. 1(b) and 1(d). The effective eigenchannel quantum defect (resonant eigen phase shifts $\pi\tau_\rho$) for the collisional channel[20–23] in the autoionization energy region for $\nu_x = 9.8$–14.1 is obtained [see Fig. 3(a)]; note that ν_x is short for the effective principal quantum number associated with threshold $3d^8(^3F)4s^4F_{9/2}$, i.e., ν_x. All the information on autoionizing states, including resonance center, width (lifetime) and configuration assignment, can be readily retrieved from this figure. First, we can directly obtain the resonance positions and widths simultaneously without relying on any fitting processes based on the isolated resonance approximation.[32,35,37,38] More specifically, the resonance centers are defined where the local maxima of the energy derivative of the eigenphase shifts appear, i.e., $\delta'_\rho = \frac{d\delta_\rho}{dE} = \frac{2\pi}{\nu_x^3}\frac{d\tau_\rho}{d\nu_x}$. At the same time, the corresponding resonance widths Γ are defined as the local maxima of the energy derivative of the eigen phase shift as follows: $\Gamma = 2/\delta'_{max}$. The characteristics of each resonance are assigned with respect to the A-coefficients obtained from Eq. (9) and use the same coloring and marker styles as in Fig. 1. We observed five open channels: $(3d^9)2D_{5/2}np_{3/2}$, $(3d^9)2D_{5/2}nf_{5/2}$, $(3d^9)2D_{5/2}nf_{7/2}$, $(3d^9)2D_{3/2}nf_{5/2}$, and $(3d^9)2D_{3/2}nf_{7/2}$, while other closed channels, associated with higher thresholds, are represented as steep rises in the phase shift at ν near integer values; the reso-

nances retrieved using the proposed method are represented by colored symbols shown in Fig. 3(a). Overlapping resonances, as a result of strong channel coupling, are found in our results. Our channel assigning technique implemented in the MQDT code allows one to separate "isolated" resonances from potentially overlapping ones. To better understand the interactions between the channels, a demonstrative zoom-in view around the region $12.8 \leq \nu_x \leq 13.05$ is provided as an inset in panel (b), and its corresponding energy derivatives of the eigen phase shifts are shown in panel (c). The first three maxima of the derivative corresponding to the denoted three states $|a\rangle$, $|b\rangle$, and $|c\rangle$ get lower as the energy increases, indicating shorter and shorter lifetimes of the three states. By analyzing the transformation matrices, we realized the third resonance is a strong mixture of $|7\rangle$ and $|8\rangle$, corresponding to $\theta_{7,8} = 0.185\pi$, while the angles for the first two resonances are much smaller. Through graphical analysis and consideration of the channel mixing coefficients, we revealed the resonance coupling mechanism and its impact on resonance width (lifetime).

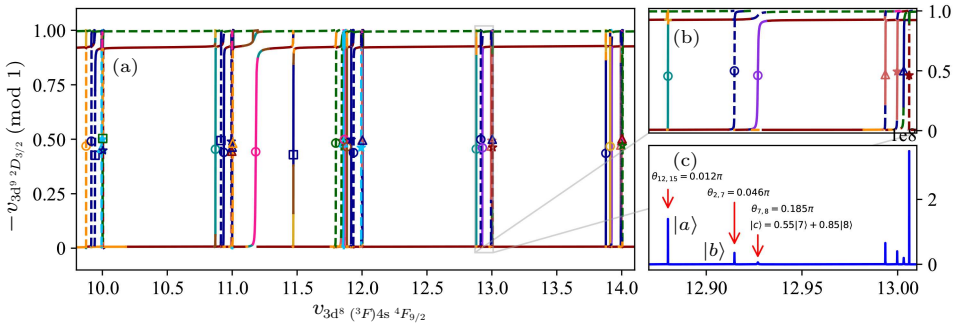


Fig. 3. (a) Graphical representation of the MQDT solutions in the autoionization energy range $9.8 \leq \nu_{3d^8 4s^4 F_{9/2}} \leq 14.1$ (corresponding to 6650 cm^{-1} < scattering energy < 7300 cm^{-1}). Panels (a) and (b) use the same coloring and marker styles as Fig. 1(c). Autoionization resonances (opened symbols) are retrieved at the steepest energy derivatives of effective eigen phase shifts. The coupling strength of the autoionizing states dictated by the Euler angle θ_k is revealed by the steepness of the avoid-crossings, as shown in panel (c).

Table 3. Comparisons of theoretical and available experimental values of resonance center as well as lifetimes of $3d^8(^3F)4s\ ^4F_{9/2}\,np_{3/2}$ and $nf_{5/2}$ autoionizing states. The resonance center shows excellent agreement with the experiment values[9,29] with a maximum deviation of 0.02%. The lifetime of resonances is compared to mean-field calculation using FAC.[40]

States	Energy levels				Lifetime (ps)	
	Theory (cm^{-1})		Experiment (cm^{-1})		This work	FAC[40]
	This work	Shi *et al.*[9]	Zhang[29]	Shi *et al.*[9]		
$3d^8(^3F)4s\ ^4F_{9/2}\ 13p_{3/2}$	68917.45		68922.02		125.843	142.287
$3d^8(^3F)4s\ ^4F_{9/2}\ 14p_{3/2}$	69107.39	69117.04		69117.93	95.529	186.356
$3d^8(^3F)4s\ ^4F_{9/2}\ 15p_{3/2}$	69252.51	69258.77		69275.47	180.597	146.448
$3d^8(^3F)4s\ ^4F_{9/2}\ 16p_{3/2}$	69364.94	69369.26		69371.11	195.798	217.884
$3d^8(^3F)4s\ ^4F_{9/2}\ 17p_{3/2}$	69454.22	69457.06	69454.84	69455.10	275.486	268.960
$3d^8(^3F)4s\ ^4F_{9/2}\ 18p_{3/2}$	69526.26	69527.98		69533.73	1156.080	205.085
$3d^8(^3F)4s\ ^4F_{9/2}\ 19p_{3/2}$	69585.30	69586.09	69585.11	69588.98	30.592	246.767
$3d^8(^3F)4s\ ^4F_{9/2}\ 20p_{3/2}$	69633.97		69634.39		13.383	293.707
$3d^8(^3F)4s\ ^4F_{9/2}\ 13f_{5/2}$	68888.29		68875.32		13.383	168.106
$3d^8(^3F)4s\ ^4F_{9/2}\ 14f_{5/2}$	69085.08		69075.68		335.661	208.960
$3d^8(^3F)4s\ ^4F_{9/2}\ 15f_{5/2}$	69236.57		69232.36		58.638	256.045
$3d^8(^3F)4s\ ^4F_{9/2}\ 16f_{5/2}$	69352.18				3132.022	309.790
$3d^8(^3F)4s\ ^4F_{9/2}\ 17f_{5/2}$	69443.91		69438.65		1395.978	370.670
$3d^8(^3F)4s\ ^4F_{9/2}\ 18f_{5/2}$	69518.53		69513.54		588.538	368.397
$3d^8(^3F)4s\ ^4F_{9/2}\ 19f_{5/2}$	69578.75		69573.12		277.248	339.604
$3d^8(^3F)4s\ ^4F_{9/2}\ 20f_{5/2}$	69629.31				297.797	257.099

The position and lifetime of autoionization resonances are important physical parameters that characterize the properties of atomic excited states. They are also key physical observables for testing the modeling of many-body effects in strongly correlated systems. This study, based on MQDT, calculates the parameters of the autoionization resonant states in the Ni atom. By comparison with experimental data[9,29] and other theoretical methods,[9] we systematically assess the reliability of the computed results and reveal the impact of electronic correlation effects on resonance lifetimes. Table 3 lists the calculated positions and lifetimes of the autoionization resonances of interest. Our results show excellent agreement with experimental measurements by Zhang *et al.*[29] with a maximum deviation of 0.007% for the resonance positions (only in the first energy level: the deviations for the rest of the levels are even one order lower). These results again demonstrated the capability of the MQDT method in the high-precision calculation of autoionization in complex atoms. We compared our calculated

lifetimes against those from a mean-field self-consistent field calculation employing the Flexible Atomic Code (FAC).[40] For the p states, fairly good agreement is found for the low-lying levels, except that the last three depart hugely from FAC values. The mean-field calculation shows a very predictable, near-monotonic increase with excitation. We attribute this striking deviation to the inclusion of correlation effects in the RMCT treatment. For the f states, more states show huge deviation from mean-field calculations. The difference in lifetime calculations highlights the advance of multichannel methods in handling electronic correlations, especially the bound–continuum correlation. They also reveal the sensitive dependence of resonance lifetimes on inter-channel interactions.

3. Summary

We applied multichannel quantum defect theory to high-precision theoretical calculation of the complex electronic structure of excited and autoionizing states of the nickel atom for $J^{\pi} = 4^{-}$ symmetry to address the surging demand in astrophysics, materials science, and energy research applications. The indispensable correlation effects between bound and continuum configurations are stringently considered by the relativistic multichannel theory (RMCT) and completely encompassed in the slow-varying scattering matrix on merely a few energy grids. Highly excited and autoionizing states are readily calculated semi-analytically with the MQDT procedure. We demonstrate the relationship of the interesting electronic correlation effects with the transformation matrices (equivalently represented by Euler angles), which consequently strongly affect the resonance width and lifetime of the physical states. Abnormal lifetime variations of the autoionizing states along the same series are observed; the origin of the abnormality is attributed to strong local electronic correlations.

Excellent agreement is achieved between the theoretical results and existing experimental discrete levels, with a maximum of 0.02 % deviation.[9,12,29] The resonance energies, lifetimes, and assignments of autoionizing states are systematically presented for the first time, with the objective of contributing to the fields of astrophysics, materials science, and energy research.

Data availability statement

The data of this study are openly available in Science Data Bank at https://doi.org/10.57760/sciencedb.j00113.00279.

Acknowledgements

R. J. is supported by the Young Scientists Fund of the National Natural Science Foundation of China (Grant No. 12404296) and the Original Exploration Program of the National Natural Science Foundation of China (Grant No. 12450404). Y.-Z. Qu is supported by the National Natural Science Foundation of China (Grant No. U2430208). S.-B. N. would like to thank Prof. Jun-Yao Zhang for fruitful discussion and sharing unpublished experimental data.

References

[1] Seaton M J, Yan Y, Mihalas D and Pradhan A K 1994 *Mon. Not. R. Astron. Soc.* **266** 805
[2] Bautista M A 1999 *Astron. Astrophys. Suppl. Ser.* **137** 529
[3] Meléndez M and Bautista M A 2005 *Astron. Astrophys.* **436** 1123
[4] Lennard W N, Whaling W, Scalo J M and Testerman L 1975 *Astrophys. J.* **197** 517
[5] Hillebrandt W and Niemeyer J C 2000 *Annu. Rev. Astron. Astrophys.* **38** 191
[6] Jorissen A 2004 *Phys. Scr.* **T112** 73
[7] Mazzali P A, Ropke F K, Benetti S and Hillebrandt W 2007 *Science* **315** 825
[8] Suzuki T, Honma M, Mao H, Otsuka T and Kajino T 2011 *Phys. Rev. C* **83** 044619
[9] Shi X, Huang H, Jacobson B and Chang Y C 2012 *Astrophys. J.* **747** 20
[10] Pain J C, Gilleron F and Comet M 2017 *Atoms* **5** 22
[11] Watson W D 1969 *Astrophys. J.* **157** 375
[12] Kessler T, Brück K, Baktash C, Beene J R, Geppert C, Havener C C, Krause H F, Liu Y, Schultz D R and Stracener D W 2007 *J. Phys. B: At. Mol. Opt. Phys.* **40** 4413
[13] Dawra D, Dimri M, Singh A K, Jha A K S, Pandey R K and Mohan M 2022 *Eur. Phys. J. D* **76** 59
[14] Mou N, Zhang X, Lin Q, Yang X, Han L, Cao L and Yang D 2023 *Nucl. Eng. Technol.* **55** 2139
[15] Gning M T and Sakho I 2024 *Phys. Part. Nucl. Lett.* **21** 1014
[16] Sardar S, Bilal M, Bari M A, Nazir R T, Hannan A, Salahuddin M and Nasim M H 2016 *Mon. Not. R. Astron. Soc.* **458** 1504
[17] Nahar S N and Bautista M A 2001 *Astrophys. J. Suppl. Ser.* **137** 201
[18] Singh J, Jha A K S and Mohan M 2010 *Astrophys. J. Suppl. Ser.* **186** 334
[19] Seaton M J 1966 *Proc. Phys. Soc.* **88** 801
[20] Lu K T 1971 *Phys. Rev. A* **4** 579
[21] Lee C M and Lu K T 1973 *Phys. Rev. A* **8** 1241
[22] Lee C M 1974 *Phys. Rev. A* **10** 584
[23] Jin R, Han X Y, Gao X and Li J M 2017 *Sci. Rep.* **7** 11589
[24] Zou Y, Tong X M and Li J M 1995 *Acta Phys. Sin.* **44** 50 (in Chinese)
[25] Xiaomin T, Yu Z and Jiaming L 1995 *Chin. Phys. Lett.* **12** 351
[26] Huang W, Zou Y, Tong X M and Li J M 1995 *Phys. Rev. A* **52** 2770
[27] Aymar M, Greene C H and Luc-Koenig E 1996 *Rev. Mod. Phys.* **68** 1015
[28] Zhang J Y, Xiong J Y, Zhou H R, Zhu C H, Sun H M, Wang L D, Chai J J and Li Y F 2025 *Spectroc. Acta Pt. B-Atom. Spectr.* **231** 107249
[29] Zhang J Y, National Key Laboratory of Particle Transport and Separation Technology, Tianjin, Private Communication
[30] Gao X and Li J M 2012 *Chin. Phys. Lett.* **29** 033101
[31] Gao X, Jin R, Zeng D L, Han X Y, Yan J and Li J M 2015 *Phys. Rev. A* **92** 052712
[32] Breit G and Wigner E 1936 *Phys. Rev.* **49** 519
[33] Wigner E P 1955 *Phys. Rev.* **98** 145
[34] Smith F T 1960 *Phys. Rev.* **118** 349
[35] Bartschat K and Burke P G 1986 *Comput. Phys. Commun.* **41** 75
[36] Peng Y L, Han X Y, Wang M S and Li J M 2005 *J. Phys. B: At. Mol. Opt. Phys.* **38** 3825
[37] Quigley L and Berrington K 1996 *J. Phys. B: At. Mol. Opt. Phys.* **29** 4529
[38] Quigley L, Berrington K and Pelan J 1998 *Comput. Phys. Commun.* **114** 225
[39] Liu J, Niu Y F and Long W H 2025 *Chin. Phys. C* **49** 064104
[40] Gu M F 2008 *Can. J. Phys.* **86** 675